TRANSMISSION MEDIUM CONSTRAINTS AND RECEIVER FRONT – END DESIGN CONSIDERATIONS FOR AN AVIONICS IR COMMUNICATION LINK

E. – O. Narlis

Hellenic Aerospace Industry
P.O. Box 23, GR – 32009, Schimatari, Greece
email: enarlis@central.ntua.gr

Abstract

This paper investigates the technological details of establishing an IR data link for aircrafts flying in close formation. First the transmission medium has been investigated. In this particular aspect the noise generating dominant parasitic sources have been identified to be the sun and the IR countermeasure flares. Second, the different architectures of front end of the communication link, which is the LNA have been extensively studied. It has been demonstrated that the common collector trans-impedance amplifier is the most suitable for this particular avionic application taking in consideration also the environmental standards, which should be met as concerns the operating temperature range. Finally the preliminary flight test for validating the operational exploitability of the system has been discussed.

1. INTRODUCTION

Modern air campaigns are carried under severe constrains which can be shortly listed as following:

1. Day and night
2. All weather
3. All altitudes
4. Keep radio silence
5. Strong jamming
6. Large number of aircrafts in close formation

Under the operational viewpoint there are some contradictory but vital requirements, which must be fulfilled in order to assure the crew safety and the success of the operations:

a. ***Contradiction 1***: Large number of aircrafts must fly and navigate in close formation (as a rigid body) during night while keeping the navigation lights off. Furthermore the flight must be carried in low altitude and nap of the earth condition.

b. ***Contradiction 2***: While the communication is vital for the success, the stealthyness imposes the radio silence in order to avoid detection.

The above requirements guided us to study and to experiment the technical feasibility of a short distance Infrared telemetry – communication link which will provide distance (in the meaning of collision avoidance) data while assuring the voice communication among the units of the formation. The infrared technology offers the capability to substitute the navigation lights and the communication contact within the formation while keeping the low probability of intercept condition.

The study will be concentrated in the investigation of the transmission medium and in the theoretical and experimental investigation of the front end IR receiver technologies.

2. TRANSMISSION MEDIUM

Two types of perturbations characterize the free air transmission medium:

a. Multipath effect due to reflections from the wings and fuselages of aircrafts of the formation

b. Solar IR emissions during day

c. Meteorological conditions such as fog, haze, rains and clouds

Examining the multipath effect (Figure 1) we can highlight that the multiple reflections will be focalized on the detector at different moments dispersing the square waveform based digital signals. This dispersion will result to inter-symbol interferences in case of high data bit rates or the parasitic phase shifts in case that the binary information modulates a carrier.

It was shown [1, 2] that multiple paths limit the maximum bit data rate to 260MBmps in order to avoid the inter-symbol interference. This means that if the airplanes of the formation fly inside of a sphere of 50m of diameter the maximum bit

data rate will be limited to 5.2Bpps. This rule of thumb is valid if the detector has a field of view of $\pm 60^0$ and the binary signal has a duty cycle of 50%.

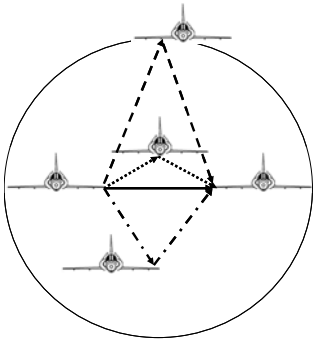

Figure 1. Multiple reflections of infrared signals from aircrafts flying in formation within a virtual sphere in space of 50m of diameter.

The parasitic sources of Near IR radiation, which fall in the mostly exploited band for IR communications, targeting and telemetry (0.7μm – 1.1μm) are the sun (during day), the laser designators, IR active countermeasure systems and the IR flares. Among the previously sited IR sources the IR active countermeasure systems and the laser target designators will not been taken in the account. In fact, although the IR countermeasure systems, which mainly use pulsed xenon, cesium or argon arc lamps (which operate between 3000 – 6000^0K) or heated rods, are very bright sources in the visible and near IR band, in practice they operate through a filter which cuts the wavelengths below 2μm. On the other side the laser designators, which emits in 1.064μm or in 1.55μm are very directive sources. Other parasitic IR sources of the operational environment such as aircraft engines have much lower operating temperatures than the previously sited sources and therefore can be neglected. It makes consequently sense to consider the sun and the flares as the dominant parasitic sources for the IR link.

2.1 MEASUREMENT OF THE NOISE POWER SPECTRAL DENSITY

In order to have a more clear understanding of the effects of the selected parasitic sources over an IR comlink we have proceeded to the measurement of the noise spectral density. The measurement setup is displayed in Figure 2. The measurement has been done first without the presence of the parasitic sources and while measuring the current generated by the ambient light of the laboratory in order to eliminate the noise generated by the ambient light and the measurement equipment. The BPW34

PIN photodiode without daylight filter is used as sensor. This diode is preferred because of its large spectral sensitivity. In the frequency domain the frequencies below 100Hz have been cut not only to eliminate any effect of the AC power supplies, but also keeping in mind that the targeting laser designators and the active IR countermeasure systems operate below 100pps. Furthermore this low cutoff would eliminate any saturation in the frequency selective modules of our measurement setup.

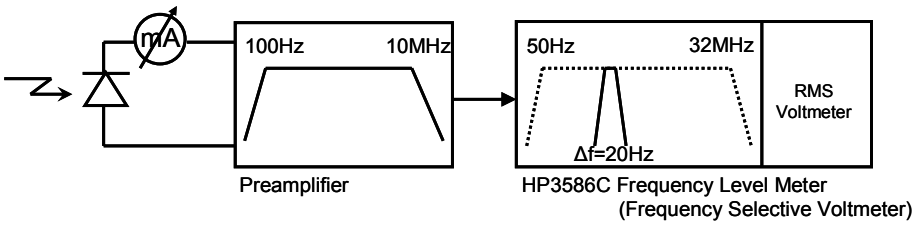

Figure 2. Setup for the measurement of the noise spectral density generated by the parasitic sources

Regarding the measurement of the noise power spectral density created in the photodiode from a flare's emission, we simulated the emission of the flare using a black body at 1m of distance from the photodiode and accordingly scaled the radiation output. This approach was considered as the most appropriate since it was not possible to ignite a flare in the laboratory and because of the absence of spectral irradiance data regarding the IR countermeasure flares. Consequently since the majority of IR countermeasure flares have a peak emission between 2 – 2.5μm we traced the Planck curve and compared with two very common flares (figure 3). Indeed, the metal powder – oxidizer flare (magnesium, sodium nitrate stoichiometric mixture) have a peak emission of $0.6 Wcm^{-2}sr^{-1}$ in the 2.3μm. The much more powerful teflon – magnesium flare (1:1 ratio of teflon and magnesium by weight) have a peak emission of $1\ Wcm^{-2}sr^{-1}$ in the 1.8μm.

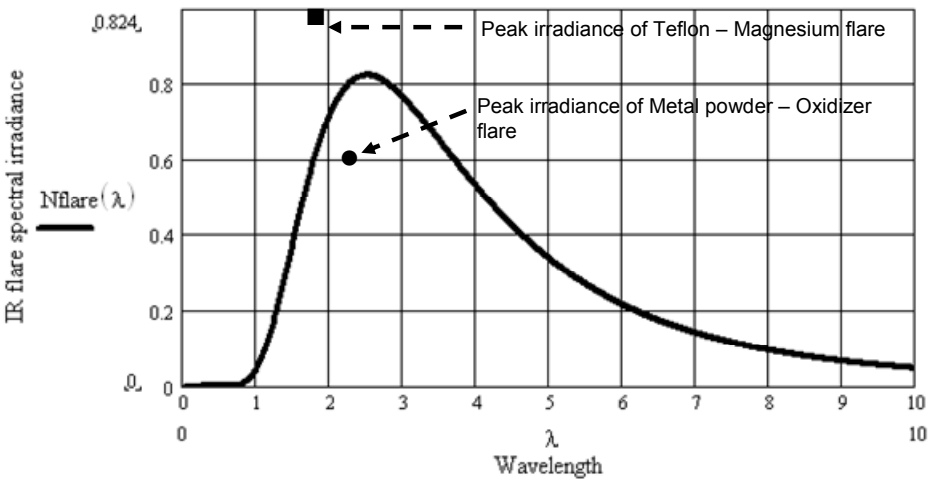

Figure 3. Theoretical spectral irradiance of a typical IR countermeasure flare. Compared to the irradiance graph the peak emissions of the metal powder - oxidizer flare and of the much more powerful teflon -magnesium flare are displayed.

The measured voltages in the absence and in the presence of the parasitic sources can analytically be displayed by the equations 1.a and 1.b. respectively.

$$V^2_{m(medium)} = G^2_A G^2_{FLM}\left(I^2_N + I^2_{SN(medium)} + I^2_A + I^2_{FLM}\right)\Delta f \qquad (1.a)$$

$$V^2_{m(parasitic)} = G^2_A G^2_{FLM}\left(I^2_N + I^2_{SN(parasitic)} + I^2_A + I^2_{FLM} + I^2_{parasitic}\right)\Delta f \qquad (1.b)$$

$V_{m(medium)}$, $V_{m(parasitic)}$: The voltage noise measured by the voltmeter in the absence and in the presence of the parasitic sources respectively.

G_A, G_{FLM}: The gain of the preamplifier and of the frequency level meter respectively.

I_N: Noise equivalent current spectral density generated by the nature.

$I_{SN(medium)}$, $I_{SN(parasitic)}$: The photodiode's shot noise spectral density in the absence and in the presence of the parasitic sources respectively.

I_A: The preamplifier's noise spectral density as transferred at the input.

I_{FLM}: The frequency level meter's noise spectral density as transferred at the input.

$I_{parasitic}$: The noise equivalent current spectral density generated by the parasitic sources themselves.

The shot noise of the photodiode can be expressed in terms of the photo-current flown through the photodiode I_Φ, such as $I^2_{SN} = 2qI_\Phi$ with q being the electron charge. Considering the facts that the ambient illumination conditions were identical during the whole measurement steps and that the laboratory equipments noise levels

are independent from the parameters of their input signals we can express the noise equivalent current spectral density of the parasitic sources as following:

$$I^2_{parasitic} = \left(\frac{V^2_{m(parasitic)} - V^2_{m(medium)}}{G^2_A G^2_{FLM} \Delta f} \right) + 2q\left(I_{\Phi(medium)} - I_{\Phi(parasitic)} \right) \quad (2)$$

The measurement results are displayed in figure 4. In the case of sun we have considered an elevation "h" approximately of 50^0 and an angle of incidence "θ" to the normal of the photodiode's surface approximately of 40^0. The results show that the flares are dominant parasitic sources even in altitudes where sun's energy rises considerably (Figure 4). However it has to be considered that operating in a sky plenty of flares is not a realistic condition. Besides the flares burnout after 15 – 20 seconds. Furthermore the need of launching flares corresponds directly to the detection and the acquisition of the friendly formation by the enemy air defense system, so it became irrelevant to keep the radio silence anymore. Under the above considerations the sun (and the moon) remains the only IR parasitic source worthy of consideration.

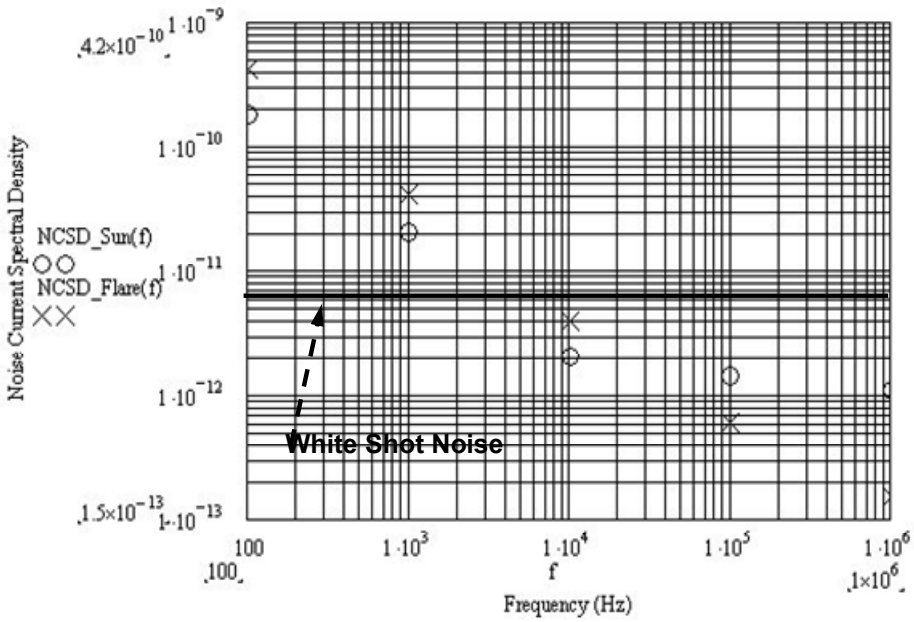

Figure 4. The measured noise equivalent current spectral densities crated by the sun and those of the simulated IR countermeasure flares. For the sun the elevation h=50^0 and the angle of incidence θ=40^0

Under the design viewpoint the surge of the colored noise due to the parasitic sources below 1KHz has to be blocked with a high pass filter having a low cutoff frequency of 1KHz. Additionally this will eliminate the DC component and consequently protect the following preamplifier stage from any saturation.

The result of the integration of the sun's spectral irradiance, as it is displayed in figure 5, over the range of the spectral sensitivity of the photodiode is the photocurrent generated by the sun:

$$I_{\Phi(Sun)} = \frac{AqC_1C_2}{hc}\int_{\lambda_1}^{\lambda_2} \lambda N(\lambda)\eta(\lambda)d\lambda \qquad (2)$$

Where q is the electron charge, h is the Planck constant, c the light velocity, A the sensitive area of the photodiode.

$C_1 = 4n/(n+1)^2$ where n is the refraction index of silicon. With n=3.44 we get C_1=0.70.

$C_2 = \cos(\theta)e^{-1/6\sin(h+2)}$ is a correction factor depending the sun's elevation h^0.

N(λ) is the spectral irradiance as displayed in figure 5, and η(λ) is the photodiode's spectral average as a function of wavelength.

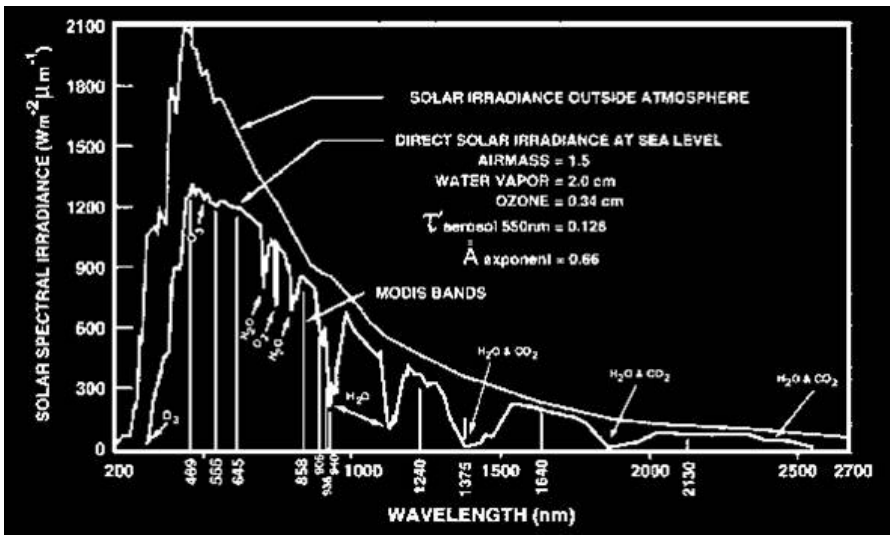

Figure 5. The sun's spectral irradiance at sea level and outside of the atmosphere.

The integration of the solar irradiance curve corresponding to the outside atmosphere between 300nm and 1200nm results to a current of 550µA/mm^2 approximately. This result corresponds to a direct illumination of the BPW34 photodiode when sun is in zenith.

2.2 ATMOSPHERIC EFFECTS ON THE IR PROPAGATION

The atmosphere acts over the IR propagation through the mechanisms of scattering and absorption. The scattering is due to the particles hovering in the atmosphere and depends to the ratio of 2πr/λ, where r is the radius of the particle and λ the wavelength. In clear atmosphere the said ratio is lower than 0.1 and for this

reason Rayleigh scattering is applied, otherwise Mie scattering is in rule. Therefore the IR propagation follows the rule of equation 3.

$$\Phi(\lambda, x) = \Phi_0(\lambda) \times e^{-k(\lambda)x} \tag{3}$$

where $\Phi(\lambda,x)$ is the light flux in distance x, $\Phi_0(\lambda)$ is the flux at the source, $k(\lambda)$ is the scattering coefficient depending to the wavelength and x is the distance from the source.

The scattering coefficient can be expressed as $k(\lambda)=8.8\text{x}10^{-3}\lambda^{-4}$ (λ in μm) [3]. For larger particles in the atmosphere where $2\pi r/\lambda \approx 0.1$, the scattering coefficient can be written as $k(\lambda)=\beta/\lambda^{\alpha}$ (λ in μm) where α and β are Angstrom coefficients.

The Angstrom coefficient "α" varies from 0 to 4 and in middle latitude zones its value is 1.3. β=0.02 for clear sky and 0.5 for overcast sky.

For particles larger than the wavelength, $k(\lambda)$ is independent to λ. In this particular case Near IR and visible light are equally attenuated [4,5]. This last case corresponds to fogs and rainfalls where the particles diameter varies from some μm to hundreds of μm.

Table 1. The approximate attenuation of visible and Near IR radiation (0.85 – 0.98μm) at sea level, depending to meteorological conditions.

METEOROLOGICAL CONDITIONS	**ATTENUATION (dB/Km)**	**ATTENUATION x = 50m**	**ATTENUATION x = 100m**
Clear weather	Negligible for visible and Near IR		
Light rainfall (0.25cm/hour)	0.4dB/km	0.46%	0.91%
Medium rainfall (1.25cm/hour)	1.8dB/km	2%	4%
Heavy rainfall (2.5cm/hour)	5.5dB/km	6.2%	12%
Light fog (visibility 850m)	40dB/km	37%	60%
Medium fog (very selective) (visibility 200m)	160dB/km	84%	98%

Interpreting table 1, it can be said that there is no significant attenuation to take into account for light rainfalls. However the attenuation must be taken into account when calculating the link budget for medium and heavy rainfalls. As concerns the fogs, it can be said that for light fog the high attenuation is of important concern, but debatable if powerful IR emitters (laser diode arrays) and avalanche photodiodes have to be used in the system. The severe attenuation caused from the medium fog, practically forbidden any IR link attempt.

It has to be noted that since these data refer to distances at sea level, for airplanes these distances must be compensated as a function of altitude. Indeed, at higher altitudes the absorption lines and bands became narrower because of the reduced pressure, and it would be expected the transmittance over a fixed path length to increase. The accompanying decrease in temperature (typically 1.98^0C/1000ft for ISA) also causes a slight increase of the transmittance. The spectral transmittance of a path having al length x_0 at sea level is equal to an equivalent path x at altitude h following the equation 4 [5].

$$x = x_0 \left(\frac{P}{P_0} \right)^{-k} \tag{4}$$

where P/P_0 is the ratio of atmospheric pressure at altitude to that at sea level. k=0.5 for water vapor

Operationally speaking, it is very unrealistic to consider close formation flights in fogs limiting so much the visibility and any attempt of near IR link connection at the limits of visibilities is doomed. In fact many authors appear very optimistic regarding the short IR transmission. The field experience demonstrates the opposite, that it is impossible to go beyond the visibility range at least as concerns field exercises with using range finders. Consequently considering a standard approximation of 12-15% attenuation for a link budget calculation appears a realistic approach covering practically the majority of the meteorological conditions where operations can be executed.

3. THE PREAMPLIFIER STAGE

The most important module of an IR comlink is the optoelectronic preamplifier stage. In the literature the type of the optoelectronic preamplifier that have been studied extensively is that of the trans-impedance type [6 – 14]. The second type that also will be considered in this study is the “Load Resistance Amplifier”. This last one is based on the amplification of the voltage across the load resistance of a photodiode.

3.1 GAIN AND BANDWIDTH ANALYSIS OF THE AMPLIFIERS

Figure 6 and figure 7 represent the structures of a Load Resistance Amplifier and of a Trans-impedance amplifier where Z_i is the input impedance, A_v is the open loop

voltage gain R_o is the output resistance of the amplifier R_L is the load resistance and R_f is the feedback resistance.

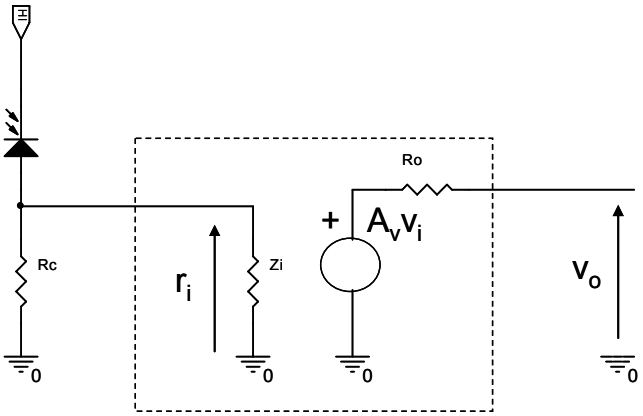

Figure 6. Load Resistance Amplifier

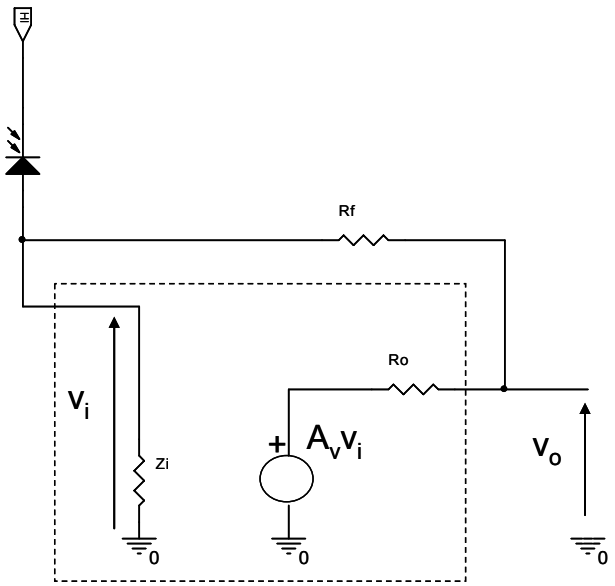

Figure 7. Trans-impedance preamplifier

It will be considered that $Z_i >> R_L$. The figures 8 and 9 display respectively the equivalent circuits of both amplifiers.

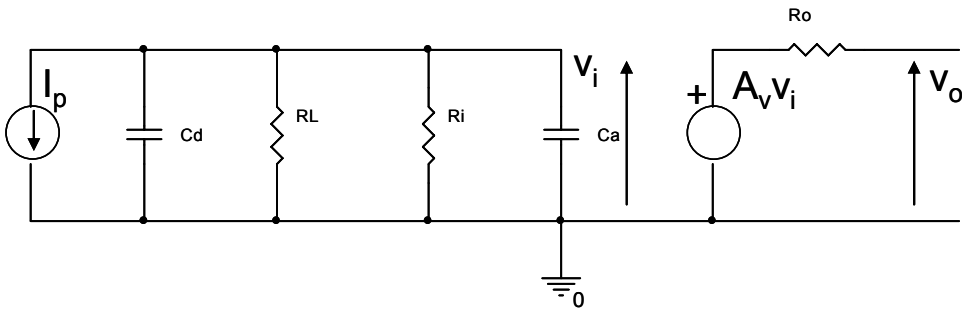

Figure 8. Equivalent circuit of the load resistance amplifier

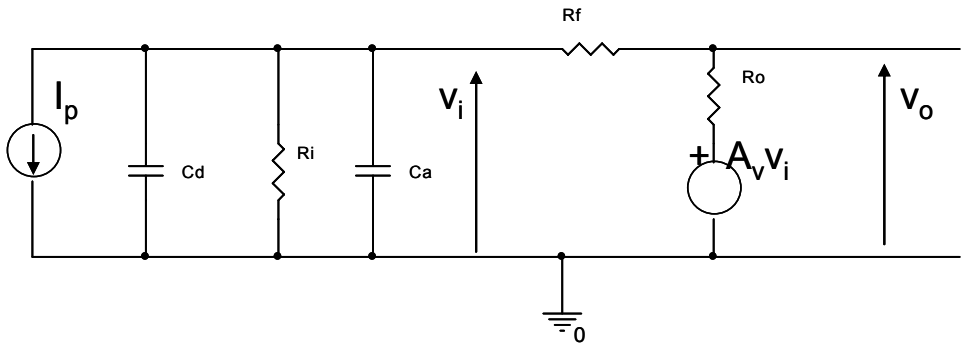

Figure 9. Equivalent circuit of the trans-impedance amplifier

where I_p is the photocurrent, C_d is the junction capacitance of the photodiode, R_i is the input resistance of the amplifier, C_a is the input capacitance of the amplifier, A_v is the open loop voltage gain and R_o is the output resistance.

Considering $R_t=(R_L//R_i)$ and $C_t=C_d+C_a$, the transfer function and the cut off frequency of the load resistance amplifier will be respectively:

$$G_\Phi\rangle_{Load\ Res\ Amplifier} = \frac{v_o}{I_p} = \frac{A_v R_t}{1 + R_t C_t p} \tag{5a}$$

$$F_c\rangle_{Load\ Res\ Amplifier} = \frac{1}{2\pi R_t C_t} \tag{5b}$$

In the same way the transfer function of the trans-impedance can be written as in equation 6.

$$G_\Phi\rangle_{Transimoedance} = \frac{v_o}{I_p} = \frac{R_i\left(A_v R_f - R_o\right)}{R_i\left(1 - A_v\right) + R_o + R_f + \left(R_o + R_f\right)R_i C_t p} \tag{6}$$

Considering $R_f >> R_o$ and $R_f/A_v R_i << 1$ the equation 6 can be simplified as following:

$$G_\Phi\rangle_{Transimpedance} \cong \frac{R_f}{1 + \frac{R_f C_t}{A_v} p} \tag{7a}$$

$$F_c\rangle_{Transimpedance} \cong \frac{A_v}{2\pi R_f C_t} \text{ being the high cut-off frequency} \tag{7b}$$

3.2 NOISE ANALYSIS OF THE AMPLIFIERS

The noise analysis has been done as reference to the noise equivalent circuits of both amplifiers, which are displayed in figures 10 and 11.

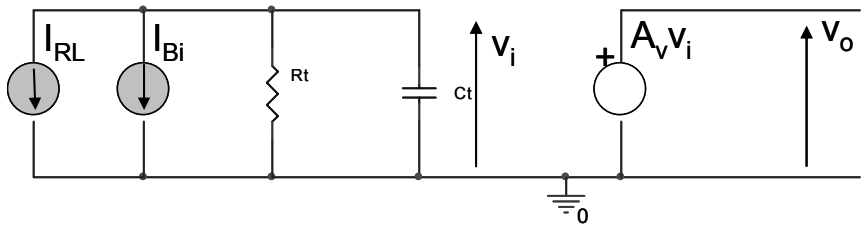

Figure 10. Noise equivalent circuit of the load resistance amplifier

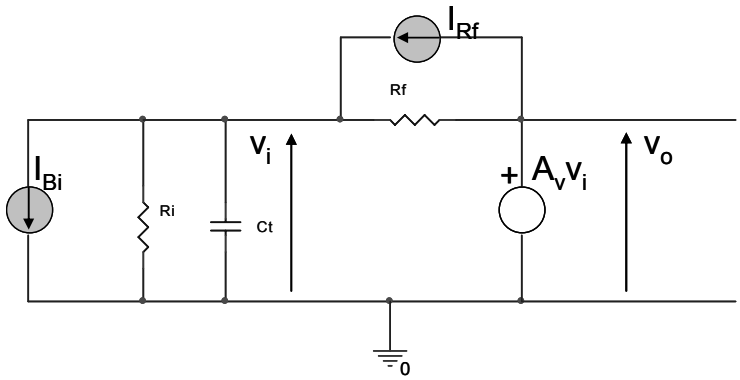

Figure 11. Noise equivalent circuit of a trans-impedance amplifier.

In both cases the noise generated by the photodiode has been neglected. This was necessary in order to evaluate the noise of each structure individually. The noise of the R_o resistance has been neglected too.

In the previous circuits I_{RL} represents the thermal noise of the load resistance R_L where the spectral density is S_{RL}= 4KT/R_L. I_{Rf} corresponds to the thermal noise of the feedback resistor R_f with spectral density S_{Rf} = = 4KT/R_f. I_{Bi} is the noise of the preamplifier referred to the input with spectral density S_{Bi}. The R_i in the circuits of figures 10 and 11 does not generate any noise because it is a virtual input resistance and so the noise of its real equivalent resistor is included in I_{Bi}. The spectral densities of the noise at the outputs of both amplifiers are given as following:

$$S_{Bout}\rangle_{Load\,Res\,Amplifier} = \frac{A_v^2 R_t^2}{\left(1 + R_t^2 C_t^2 \omega^2\right)}\left(S_{RL} + S_{Bi}\right) \tag{8a}$$

$$S_{Bout}\rangle_{Transimppedancer} = \frac{R_f^2}{\left(1 + \frac{R_f^2 C_t^2}{A_v^2}\omega^2\right)}\left(S_{Rf} + S_{Bi}\right) \tag{8b}$$

In order to compare the noise generated from the amplifiers we will consider that both amplifiers are of equal bandwidths, which are necessary to restitute the original signal without degradation. The equations 5 and 6 impose the following relations:

$$R_{t(1)}C_{t(1)} = \frac{R_{f(2)}C_{t(2)}}{A_{v(2)}} \tag{9a}$$

$$R_{f(2)} = A_{v(1)}R_{t(1)} \tag{9b}$$

where the indexes (1) and (2) refer to the Load Resistance Amplifier and to the Trans-impedance Amplifier respectively.

Assuming that for both circuits the same photodiode is used and that both circuits have the same front-end architecture (i.e. cascode, common collector or common emitter), then for both circuits the photodiode junction capacitances will be equal ($C_{d(1)}=C_{d(2)}$). The same is true for both amplifier's input capacitances ($C_{a(1)}=C_{a(2)}$). Then for equations 9, both circuits will have the same transfer function if $R_{f(2)}=A_{v(2)}R_{t(1)}$ and $A_{v(2)}=A_{v(1)}$. Generally $R_{L(1)}<<Z_{i(1)}$ is a correct assumption so $R_{L(1)}\approx R_{t(1)}$

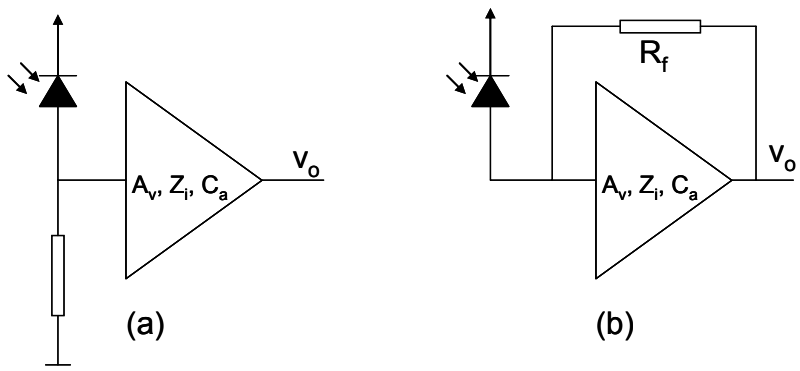

Figure 12. Two amplifier structures realizing the same transfer function

Regarding the saturation, both circuits present identical dynamic ranges. The maximum dynamic of the photocurrent is $\left|I_p\right|_{\max} \leq \frac{V_{cc}}{R_f}$. However the bias of the photodiode as displayed in figure 12.b is preferable. In fact, in this particular circuit, the voltage across the photodiode's leads remains stable independently to the photocurrent level. The anode voltage of the photodiode depends strongly to the operation point of the following amplifier, an operating point, which remains independent to the continuous photocurrent. The voltage across the leads of R_f is the parameter, which varies as a function of the photocurrent. The contrary is true for the circuit of figure 12.a. Indeed the photodiode's anode voltage is in linear dependence to the continuous photocurrent, resulting to a variation of the reverse bias of the

photodiode and consequently resulting to a bandwidth modification as a function of the received optical intensity.

Substituting the R_L term with R_f/A_v in equations 8.a and 8.b we obtain:

$$S_{Bout}\rangle_{Load\,Res\,Amplifier} = \frac{R_f^2}{\left(1+\frac{R_f^2 C_t^2}{A_v^2}\omega^2\right)}\left(\frac{4KTA_v}{R_f}+S_{Bi}\right) \tag{10a}$$

$$S_{Bout}\rangle_{Transimppedancer} = \frac{R_f^2}{\left(1+\frac{R_f^2 C_t^2}{A_v^2}\omega^2\right)}\left(\frac{4KT}{R_f}+S_{Bi}\right) \tag{10b}$$

Since both amplifiers have equal open loop characteristics (meaning that the noise spectral densities referred to the inputs S_{Bi} remain the same for both circuits) the equations 10a and 10b show that the thermal noise of the R_L resistor is A_v times larger then that of the R_f. It is concluded accordingly that the trans-impedance circuit is less noisy. These results are in accordance with previous researches [15, 16] where the condition for minimum noise implies that R_L and R_f must have the maximum possible value.

3.3 NOISE AND BANDWIDTH CONSIDERATIONS OF CE, CC AND CAS FRONT-ENDS

Figures 13, 14 and 15 display the three architectures we will invesatigate. The last stage is a common collector stage in order to have low output impedance R_o. The feedback can be placed two ways. One way is to connect the R_f across the input and the output of the second stage (i. e. the base of the transistor which constitutes the last common collector), or across the input and the output of the circuit. In fact it will be shown later that the connection of the feedback resistor is practically irrelevant to the stability conditions.

The noise analysis will be carried out by calculating the equivalent noise current transferred to the input. The noise of the photodiode and of the transmission medium will be neglected in order to isolate the noise of each structure.

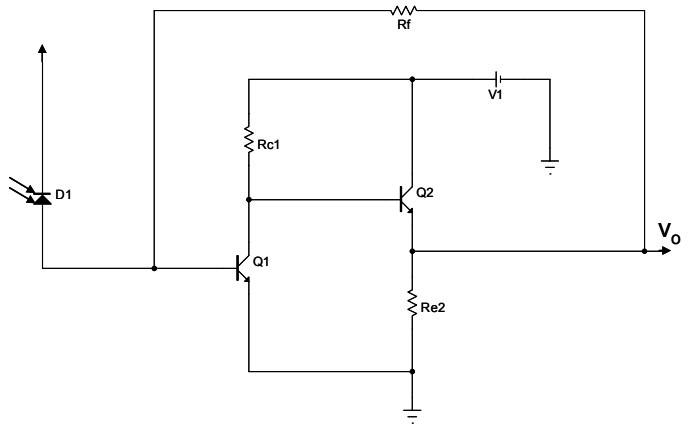

Figure 13. Common Emitter (CE) front-end

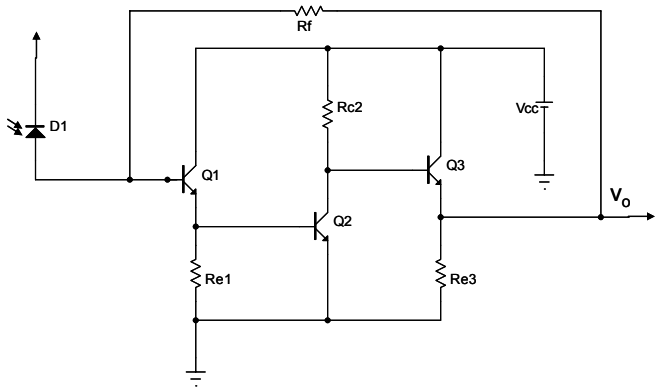

Figure 14. Common Collector (CC) front-end

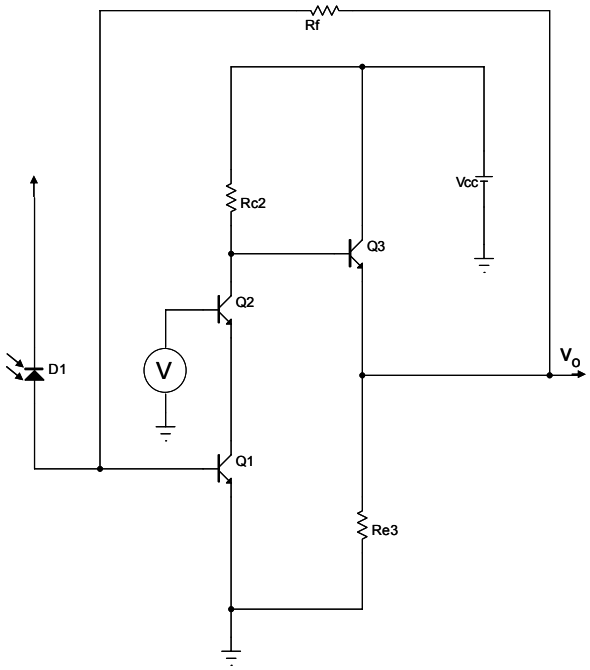

Figure 15. Cascode (CAS) front-end

3.3.1 COMMON EMITTER FRONT-END

The noise equivalent circuit of the common emitter front-end is displayed in figure 16.

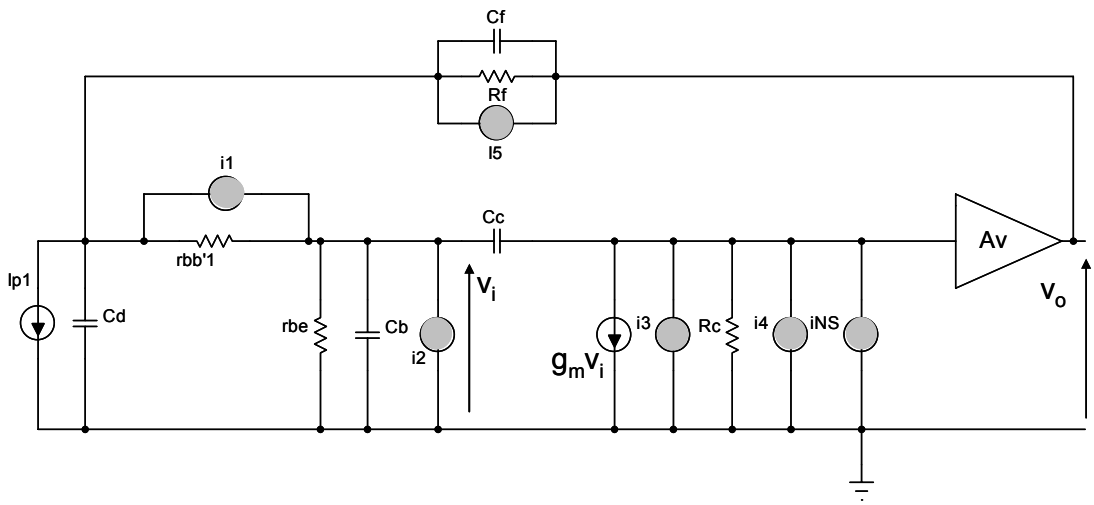

Figure 16. Equivalent circuit of CE transimpedance amplifier

$r_{bb'}$: Base input resistance of the first stage
$r_{b'e}$: Dynamic input resistance = V_T/I_B, where I_B is the base bias current
C_b: Base – emitter capacitance and C_c; base – collector capacitance
g_m: Transistor's slope = I_C/V_T, where I_C is the collector's bias current
R_c: Collector resistor
A_v: Open loop gain of the following stages
I_1^2: $r_{bb'}$ thermal noise with spectral density $4KT/ r_{bb'}$
I_2^2: Shot noise generated by I_B with spectral density $2qI_B$
I_3^2: Shot noise generated by I_C with spectral density $2qI_C$
I_4^2: R_C thermal noise with spectral density $4KT/ R_C$
I_5^2: R_f thermal noise with spectral density $4KT/ R_f$
I_{NS}^2: Noise generated by the following stages with spectral density of S_{NS}
I_p: Photocurrent
C_f: The parasitic capacitance of the feedback resistor
We will consider that $C_i = C_d+C_b+C_c+C_f$

The spectral noise density of the total noise transferred to the input is:

$$S_{CE} = 4KTr_{bb'}\left(\frac{1}{R_f^2}+C_d^2\omega^2\right)+2qI_B+\frac{4KT}{R_f}+\left(S_{NS}+2qI_C+\frac{4KT}{R_C}\right)\frac{1}{g_m^2}\left[\left(\frac{1}{R_f}+\frac{1}{r_{b'e}}\right)^2+C_i^2\omega^2\right] \tag{11}$$

Assuming that $r_{bb'} << R_f$ and $g_m R_C >> 1$ then we have:

$$S_{CE} = \left[\frac{4KT}{R_f} + 2qI_B + \left(\frac{1}{R_f} + \frac{1}{r_{b'e}} \right)^2 \left(\frac{2qV_T^2}{I_C} + \frac{S_{NS}V_T^2}{I_C^2} \right) \right] + \omega^2 \left[4KTr_{bb'}C_d^2 + \frac{2qC_i^2V_T^2}{I_C} + \frac{S_{NS}V_T^2C_i^2}{I_C^2} \right] \tag{12}$$

Evolving the equation 7.b for the this particular circuit, the cutoff frequency of the common emitter amplifier will be:

$$f_{c(CE)} = \frac{A_v g_m R_C}{2\pi R_f \left[C_d + C_b + (g_m R_C + 1)C_C + g_m R_C A_v C_f \right]} \tag{13}$$

The C_t term of equation 7b will be substituted with $C_t=C_d+C_b+C_m$ where C_m is the miller capacitance at the input of the amplifier, $C_m=C_c(1+g_mR_C)$.

3.3.2 COMMON COLLECTOR FRONT-END

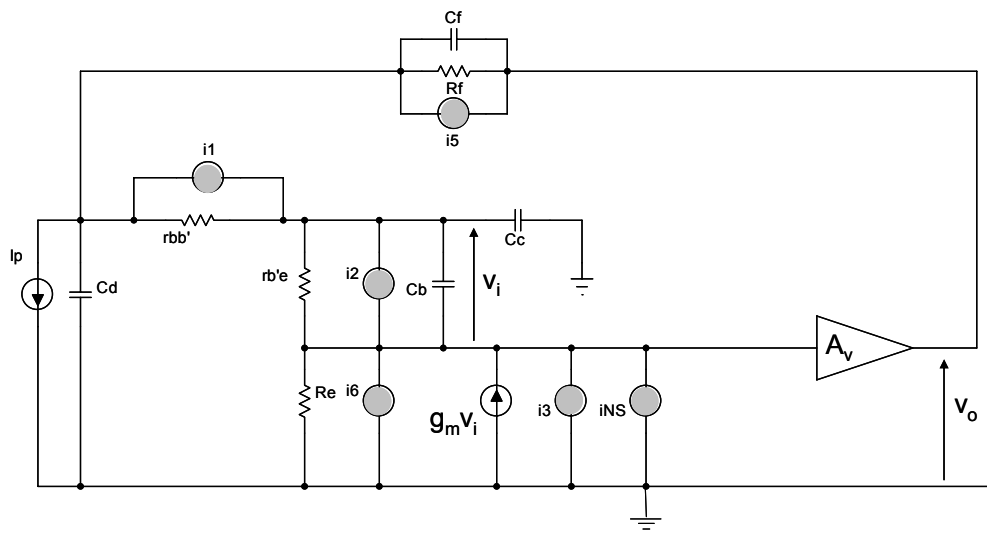

Figure 17. Equivalent circuit of CC trans-impedance amplifier

The i_6^2 current source corresponds to the noise generated by the emitter resistor and its spectral density is $4KT/R_e$.

After having transferred all the noise sources in the input the spectral noise density will be:

$$S_{CC} = \left[\frac{4KT}{R_f} + 2qI_B + \left(\frac{2qV_T^2}{I_C} + \frac{4KTV_T^2}{R_eI_C^2} + \frac{S_{NS}V_T^2}{I_C^2} \right) \left(\frac{1}{R_f} + \frac{1}{r_{b'e}} \right)^2 \right] + \omega^2 \left[4KTr_{bb'}C_d^2 + \left(\frac{2qV_T^2}{I_C} + \frac{4KTV_T^2}{R_eI_C^2} + \frac{S_{NS}V_T^2}{I_C^2} \right) C_i^2 \right] \tag{14}$$

The term $4kTV_T^2/R_eI_C^2$ compared to $2qV_T^2/I_C$ it can be neglected. This is because R_eI_c voltage will be always much higher than V_T.

It has to be noted that in the CC architecture the first stage voltage gain is equal to "1" and since the next stage is a CE we must consider also the noise contribution of the next stage. The dominant parameters of noise of the next stage will be the base input resistance and the B-E junction shot noise. Index 1 will correspond to the parameters of the CC stage (the 1st. one) and index 2 will correspond to the CE stage (the 2nd one).

In the following equation $C_{in1}=C_d+C_{c1}$ corresponds to the input capacitance of the first stage and $R_{in1}=r_{bb'1}+r_{b'e1}+\beta[R_{e1}//(r_{bb'2}+r_{b'e2})]$ corresponds to the input resistance of the first stage. Then the spectral noise density of the second stage transferred to the input will be [6]:

$$S_{NS} = rKTr_{bb'2}\left[\left(\frac{1}{R_f}+\frac{1}{R_{in1}}\right)^2 + C_{in1}^2\omega^2\right] + \frac{2qI_{B2}}{g_{m1}^2}\left[\left(\frac{1}{R_f}+\frac{1}{r_{b'e1}}\right)^2 + C_i^2\omega^2\right] \quad (15)$$

Importing equation (15) into equation (14) and considering $r_{bb'2}<<R_f$ and $I_{B2}<<I_{C1}$ the noise spectral density of the circuit is obtained as following:

$$S_{CC} = \left[\frac{4KT}{R_f} + 2qI_{B1} + \left(\frac{1}{R_f}+\frac{1}{r_{b'e1}}\right)^2 \frac{2qV_Y^2}{I_{C1}}\right] + \omega^2\left(4KTr_{bb'1}C_c^2 + 4KTr_{bb'2}C_{in1}^2 + \frac{C_i^2\, 2qV_T^2}{I_{C1}}\right) \quad (16)$$

The cutoff frequency of the common collector amplifier can be obtained by:

$$f_{c(CC)} = \frac{A_v}{2\pi R_f\left(C_d + C_{c1} + \frac{1}{\beta}C_{in2} + A_v C_f\right)} \quad (17)$$

In equation (17) $C_{in2}=C_{b2}+(A_v+1)C_{c2}$.

3.3.3 CASCODE FRONT-END

The equivalent circuit of the cascade amplifier is displayed in figure 18. The index 1 corresponds to the first transistor and the index 2 corresponds to the common base connected transistor. The terms i_7^2 and i_{10}^2 represent the thermal noises of $r_{bb'2}$ and of R_{c2} respectively. The terms i_8^2 and i_9^2 correspond to the shot noise of the bias currents I_{B2} and I_{C2} respectively.

The spectral density of the noise transferred to the input S_{CAS} is:

$$S_{CAS} = \frac{4KT}{R_f} + 2qI_B + 4KTr_{bb'1}\left(\frac{1}{R_f^2} + C_d^2\omega^2\right) + \frac{4KT}{R_{c2}g_{m1}^2} +$$
$$+\left[\left(\frac{1}{R_f} + \frac{1}{r_{b'e1}}\right)^2 + C_i^2\omega^2\right]\left[\frac{2qI_{C1}}{g_{m1}^2} + \frac{2qI_{B2}}{g_{m1}^2} + \frac{S_{NS}}{g_{m1}^2} + \frac{2qI_{C2}}{g_{m1}^2 g_{m2}^2}\left(\frac{1}{r_{b'e2}^2} + C_{b2}^2\omega^2\right)\right] \quad (18)$$

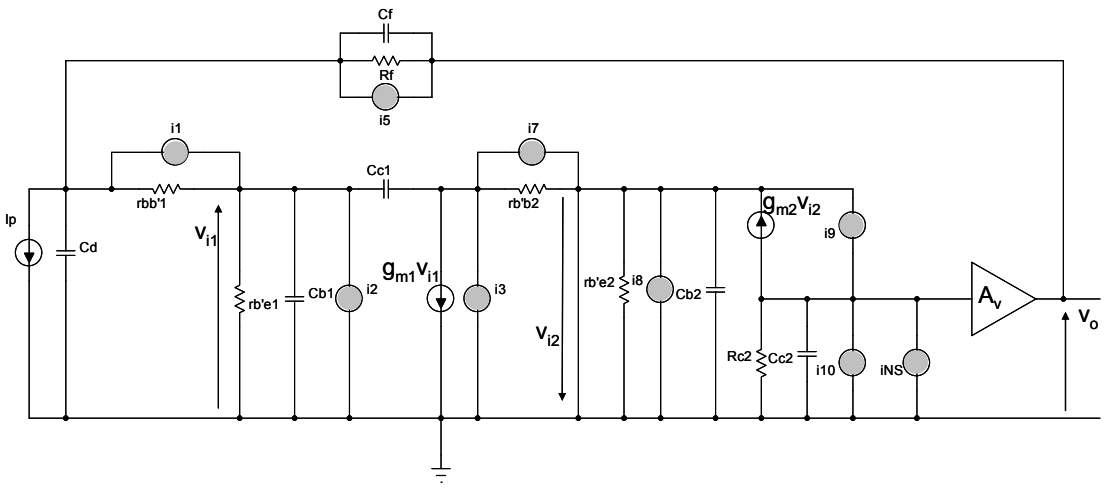

Figure 18. Equivalent circuit for CAS trans-impedance amplifier

Assuming that $I_{C1} \approx I_{C2}$, $R_f >> r_{bb'1}$ and $g_{m1}R_c >> 1$ the equation (18) is evolved to:

$$S_{CAS} = \left[\frac{4KT}{R_f} + 2qI_{B1} + \left(\frac{1}{R_f} + \frac{1}{r_{b'e1}}\right)^2\left(\frac{2qV_T^2}{I_{C1}} + \frac{S_{NS}V_T^2}{I_{C1}^2}\right)\right] +$$
$$+\omega^2\left(4KTr_{bb'1}C_d^2 + \frac{2qV_T^2C_i^2}{I_{C1}} + \frac{S_{NS}V_T^2C_i^2}{I_{C1}^2}\right) \quad (19)$$

Accordingly the cutoff frequency of the cascade circuit is given by:

$$f_{c(CAS)} = \frac{A_v}{2\pi R_f\left(C_d + C_{b1} + 2C_{c1} + A_vC_f\right)} \quad (20\}$$

It is worthy of attention that in all cutoff frequency expressions (i. e. equations 13, 17 and 20) the parasitic capacitance C_f is transferred to the input multiplied by a factor of A_v. Therefore this capacitance must be minimized by all means. The circuit board technology has an essential role to play for this particular issue which is of prime importance for the bandwidth.

3.4 STABILITY ANALYSIS FOR TRANS-IMPEDANCE CIRCUITS

Since the trans-impedance amplifier is a fed back system the stability is one of the critical points of the design.

If the output resistance R_o compared to R_f has to be neglected, if the photodiode's input capacitance C_d is considered to be the dominant parameter of the total input capacitance C_t, and instead of R_i the complex input impedance $Z_i' = R_i//C_d$ is placed in equation 6, then the said equation can be written as:

$$G_{\Phi}\rangle_{transimpedance} = \frac{v_o}{I_p} = \frac{A_v R_f Z_i'}{Rf + Z_i'(1 - A_v)} \tag{21}$$

This equation can be also written as:

$$G_{\Phi}\rangle_{transimpedance} = \frac{v_o}{I_p} = \frac{-\left(\dfrac{-A_v R_f Z_i'}{R_f + Z_i'}\right)}{1 + \left(\dfrac{-A_v R_f Z_i'}{R_f + Z_i'}\right)\left(\dfrac{1}{R_f}\right)} \tag{22}$$

Where in simplified form:

$$G_{\Phi}\rangle_{transimpedance} = \frac{v_o}{I_p} = \frac{A(p)}{1 + A(p)\beta(p)} \tag{23}$$

where $A(p) = -\dfrac{A_v R_f Z_i'}{R_f + Z_i'}$ and $\beta(p) = 1/R_f$ (24)

of a feedback system

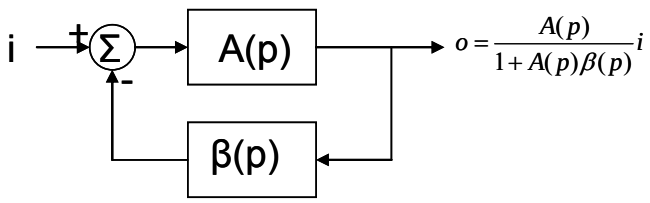

Figure 19. The model of a trans-impedance amplifier

Since A_v gain is negative the transmittance $A(p)\beta(p)$ can be written as:

$$A(p)\beta(p) = -\frac{A_v}{R_f}\left[Z_i // R_f // \left(\frac{1}{C_d p}\right)\right] \tag{25}$$

The investigation for stability of the system can be performed using the phase margin criterion for the transmittance function A(p)β(p). In fact this last expression corresponds to a linear open loop system (fig. 20)

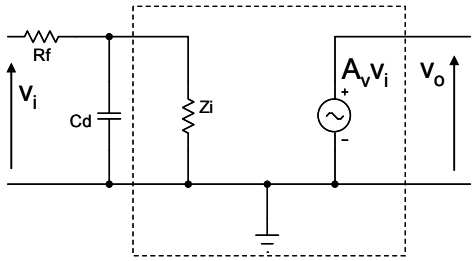

Figure 20. Equivalent circuit of A(p)β(p)

For the three circuits the poles of their respective transmittance function will be investigated. This will lead us to position comparatively the respective phase margins of the three circuits. Taking as a basis the model circuit of figure 20, we will expand it for each of our circuits. Also in our investigation we will systematically add a zero corresponding to $\omega_c=1/R_fC_f$ in order to include the effect of the parasitic feedback capacitance.

3.4.1 COMMON EMITTER CIRCUIT STABILITY MODEL

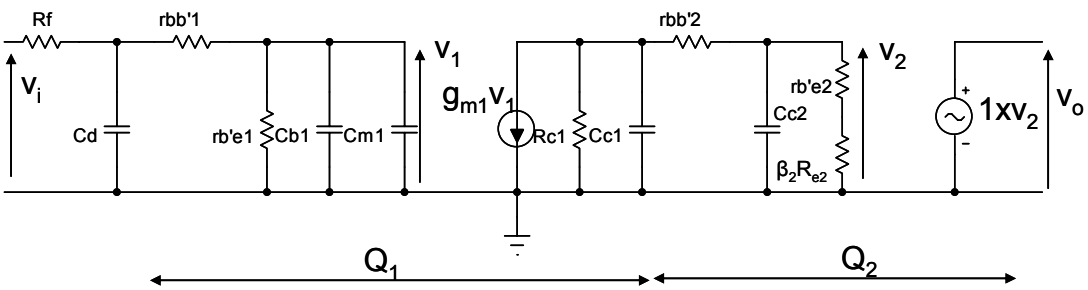

Figure 21. Stability model circuit for common emitter

The circuit in figure 21 is the CE counterpart of the figure 20. C_{m1} represents the Miller capacitance of the first stage and its value is $(1+g_{m1}R_{c1})C_{c1}$.

$$\omega_{c1} = \frac{1}{R_f // r_{b'e1}\left(C_d + C_{b1} + C_{m1}\right)} \tag{26a}$$

$$\omega_{c2} = \frac{C_d + C_{b1} + C_{m1}}{r_{bb'1}C_d\left(C_{b1} + C_{m1}\right)} \tag{26b}$$

$$\omega_{c3} = \frac{1}{2R_{c1}C_{c1}} \tag{26c}$$

$$\omega_{c4} = \frac{2}{r_{bb'2} C_{c1}} \tag{26d}$$

3.4.2 COMMON COLLECTOR CIRCUIT STABILITY MODEL

Departing from the equivalent circuit of figure 22 the transmittance poles are:

$$\omega_{c1} = \frac{1}{R_f^{'} C_t} \text{ where } C_t=C_d+C_{c1} \text{ and } R_f^{'}=R_f//R_{in1} \text{ and } Rin1=R_{b'e1}+\beta R_{e1} \tag{27a}$$

$$\omega_{c2} = \frac{1}{\left(r_{bb'2} + \frac{1}{g_{m1}}\right) C_{in2}} \text{ where } C_{in2}=C_{b2}+(1+g_{m2}R_{c2})C_{c2} \tag{27b}$$

$$\omega_{c3} = \frac{1}{2R_{c2} C_{c2}} \tag{27c}$$

$$\omega_{c4} = \frac{2}{r_{bb'3} C_{c3}} \tag{27d}$$

$$\omega_{c5} = \frac{1}{r_{bb'1} C_{c1}} \tag{27e}$$

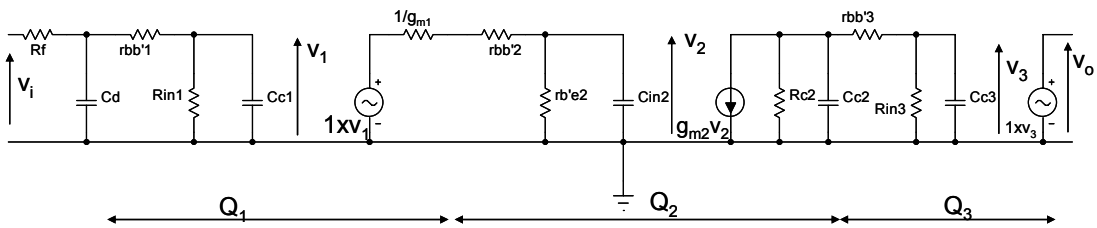

Figure 22. Stability model circuit for common collector

3.4.3 CASCODE CIRCUIT STABILITY MODEL

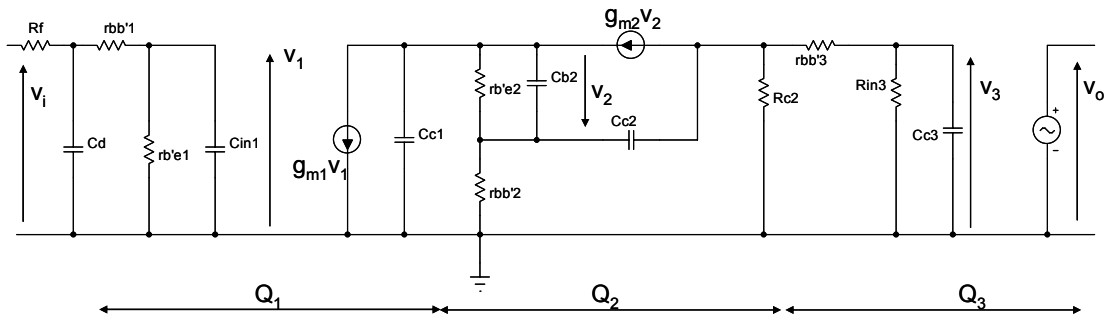

Figure 23. Stability model circuit for cascode ($R_{in}=r_{b'e3}+\beta R_{e3}$)

Departing from the circuit of figure 23 the transmittance function of the cascode circuit has the following poles:

$$\omega_{c1} = \frac{1}{R_f^{'} C_t} \text{ with } C_t=C_d+C_{in1} \text{ (where } C_{in1}=C_{b1}+2C_{c1}) \text{ and } R_f^{'}=R_f//r_{b'e1} \tag{28a}$$

$$\omega_{c2} = \frac{C_t}{r_{bb'1} C_d C_{in1}} \tag{28b}$$

$$\omega_{c3} = \frac{1}{2R_{c2} C_{c2}} \tag{28c}$$

$$\omega_{c4} = \frac{2}{r_{bb'3} C_{c3}} \tag{28d}$$

$$\omega_{c5} = \frac{g_{m2}}{C_{c1} + C_{b2}} \tag{28e}$$

3.4.4 COMPARATIVE POSITIONING OF THE PHASE MARGINS OF THE THREE TRANS-IMPEDANCE AMPLIFIERS

In order to compare the phase margins of each one of the three previously described architectures, it is needed to investigate the relative positions of the poles of each circuit on the ω axis. In fact the dominant pole, which is this that defines the bandwidth, is the ω_{c1}, carries the effect of the photodiode capacitance C_d, being the highest capacitance of the circuit. The pole ω_{c1} creates a slope of 20dB/dec on the transfer function which cuts the 0dB axis in the frequency of ω_{c0}. Therefore more the next poles ω_{c2}, ω_{c3}, etc… are closer to the ω_{c0}, more the phase margin of the circuit will be reduced.

For all three circuits the ω_{c0} gets the same value, which is equal to the high cutoff frequency ω_{FB} of the closed loop circuit, since it is needed to compare the stability for the same bandwidth for all three circuits.

$$(\omega_{co})_{CE} = (\omega_{co})_{CC} = (\omega_{c0})_{CAS} = \frac{A_v}{R_f C_t} \cong \omega_{FB} \tag{29}$$

The calculations have been done considering that the transistors for all three circuits are fully identical regarding their junction capacitances, forward current gains and their spreading resistances. Considering that $C_b=\Lambda_1 C_c$ and $C_d=\Lambda_2 C_b$ we can calculate the following ratios:

$$\frac{\omega_{c2}}{\omega_{o0(CE)}} = \frac{1+\Lambda_1}{r_{bb'1}\omega_{FB}\Lambda_1\Lambda_2 C_c\left(1+\omega_{FB}R_f C_c \Lambda_2\right)} \tag{30}$$

$$\frac{\omega_{c3}}{\omega_{o0(CE)}} = \frac{1}{2R_{c1}\omega_{FB}C_c} \tag{31}$$

$$\frac{\omega_{c2}}{\omega_{o0(CC)}} = \frac{1}{r_{bb'2}\omega_{FB}C_c\left(\Lambda_1 + \omega_{FB}R_f C_c\left(1+\Lambda_1\Lambda_2\right)\right)} \tag{32}$$

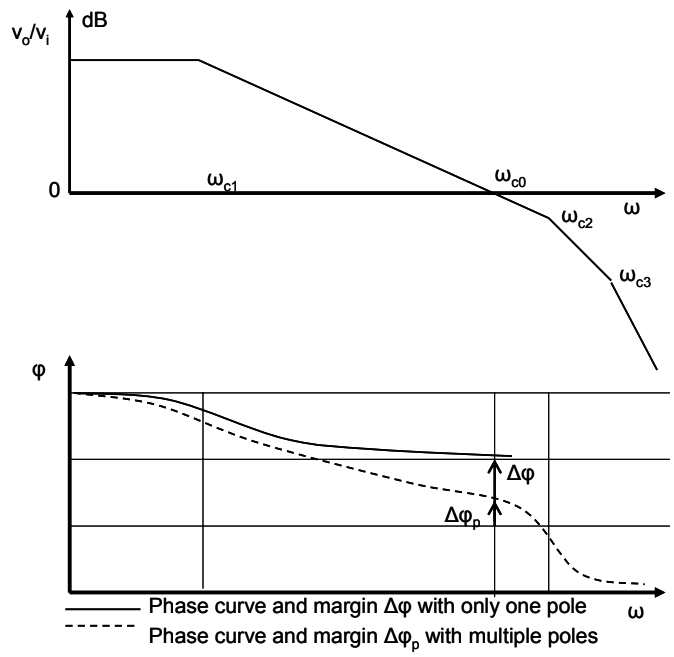

Figure 24. Phase curve and phase margin analysis

$$\frac{\omega_{c3}}{\omega_{o0(CC)}} = \frac{1}{2R_{c2}\omega_{FB}C_c} \tag{33}$$

$$\frac{\omega_{c2}}{\omega_{o0(CAS)}} = \frac{2+\Lambda_1+\Lambda_1\Lambda_2}{r_{bb'1}\omega_{FB}C_c(2+\Lambda_1)\Lambda_1\Lambda_2} \tag{34}$$

$$\frac{\omega_{c3}}{\omega_{o0(CAS)}} = \frac{1}{2R_{c2}\omega_{FB}C_c} \tag{35}$$

Since the ω_{c4} and ω_{c5} frequencies are much distant from the ω_{c2} and ω_{c3} ones their contribution to the phase margin is insignificant and therefore they have been neglected for all three cases. From the equations 31 – 36 the general conclusion is that ω_{c2} of the common emitter and that of the common collector are very close. The ω_{c2} of the cascode is more distant than that of the respective pole of the other circuits. ωc3 is the same for all three circuits. Considering that: $A_{v(CE)}>A_{v(CAS)}>A_{v(CC)}$ we can deduce that $\omega_{c3(CC)}>\omega_{c3(CAS)}>\omega_{c3(CE)}$. For the previous deductions it was assumed that R_cs of the three circuits have been selected such way to keep the transistor slopes g_ms identical for all circuits. This means that the collector currents I_c were kept equal resulting o the same noise spectral densities for all the transistors. The above results lead us to the conclusion that the common collector circuit and the cascode circuit have more stability margins than the common emitter one. Now comparing the common collector with the cascode it appears that in theory the cascode could have an advantage over the common collector one, depending how

distant could be the cascode's ω_{c2} pole. However it will be shown later that this last criterion is mostly misleading if the technology variations and environmental constrains would be neglected.

3.4.5 THE NOISE GENERATED BY THE THREE AMPLIFIERS – COMPARATIVE ASSESSMENT

It has been shown in the previous paragraphs that the stability and the noise are closely related to each other. Indeed when the circuits are operated with high bias currents some poles of the transmittance function are pushed toward higher frequencies increasing simultaneously the noise. The equations 12, 16 and 19 can be rewritten, this time considering that the noise generated by the next stages is negligible, meaning S_{NS}=0.

$$S_{CE} = \left[\frac{4KT}{R_f} + 2qI_{B1} + \left(\frac{1}{R_f} + \frac{1}{r_{b'e1}}\right)^2 \frac{2qV_T^2}{I_{C1}}\right] + \left(4KTr_{bb'1}C_d^2 + \frac{2qC_i^2V_T^2}{I_{C1}}\right)\omega^2 \tag{36}$$

$$S_{CE} = \left[\frac{4KT}{R_f} + 2qI_{B1} + \left(\frac{1}{R_f} + \frac{1}{r_{b'e1}}\right)^2 \frac{2qV_T^2}{I_{C1}}\right] + \left(4KTr_{bb'1}C_d^2 + 4KTr_{bb'2}C_{in1}^2 + \frac{2qC_i^2V_T^2}{I_{C1}}\right)\omega^2 \tag{37}$$

$$S_{CAS} = \left[\frac{4KT}{R_f} + 2qI_{B1} + \left(\frac{1}{R_f} + \frac{1}{r_{b'e1}}\right)^2 \frac{2qV_T^2}{I_{C1}}\right] + \left(4KTr_{bb'1}C_d^2 + \frac{2qC_i^2V_T^2}{I_{C1}}\right)\omega^2 \tag{38}$$

The above equations have to be integrated over the bandwidth, then substituting all I_{B1}s by I_{C1}/β and after differentiation there will be found that there is an optimum collector bias current I_{Copt} which minimises the three previous equations:

$$I_{Copt} = 2\pi V_T C_i B\sqrt{\frac{\beta}{3}} \tag{39}$$

where B is the bandwidth, β is the forward current gain of the transistors and C_i=C_d+C_b+C_c+C_f. It should be noted that C_b has considered independent from I_c.

The equations 37 – 38 can be integrated over the signal bandwidth after having substituted the I_{C1} current with their optimum values (equation 39):

$$\int_B S_{CE} = \frac{B^2 8qV_T C_i \pi}{\sqrt{3\beta}} + \frac{4KTB}{R_f} + 4KTr_{bb'1}C_d^2 B^3 \frac{(2\pi)^2}{3} \tag{40}$$

$$\int_B S_{CC} = \int_B S_{CE} + 4KTr_{bb'2}C_{in1}^2 B^2 \frac{(2\pi)^2}{3} \tag{41}$$

$$\int_B S_{CAS} = \int_B S_{CE} \tag{42}$$

It is clear that the common emitter and the cascade have the same noise characteristics for equal optimum collector bias current. The common collector circuit will be more "noisy" than the others because of the resistance $r_{bb'2}$. However for bandwidths in the order of tens of MHz and/or for low $r_{bb'}$ values of the order of hundred of ohms the second component of the equation 42 can be neglected and therefore it is conceivable to consider both cascade and common collector circuits equivalent for their noise.

3.5 EXPERIMENTAL RESULTS ON THE THREE PREAMPLIFIER STAGES

3.5.1 BEHAVIOUR OF THE PREAMPLIFIER CIRCUITS TO THE VARIATION OF B

The variation of β changes the $r_{b'e}$ values. In fact following the equations 26a, 27a and 28a only the ω_{c1} poles of the common emitter and of the cascade change. On the other side common collector appears to be invariant.

It is worthy to notice that the stability of the cascade decrease considerably by increasing β. In fact, a higher value of β will causes the augmentation of the $r_{bb'}$, which is the main cause of the decrease of the stability.

3.5.2 INFLUENCE OF THE Cb CAPACITANCE ON THE BEHAVIOUR OF THE THREE CIRCUITS

There is a slight tendency of the cascode amplifier to be somehow destabilized. In reality all of the three circuits are affected, but this effect is more visible at the cascode circuit.

3.5.3 INFLUENCE OF THE $r_{BB'}$ RESISTANCE

In paragraph 3.5.1 it has been shown that a higher β transistor means a transistor with higher rbb' which destabilizes the circuits In fact the cascode is the

most susceptible to this effect. Practically speaking, the common collector is the circuit which appears to be more stable against $r_{bb'}$ variations.

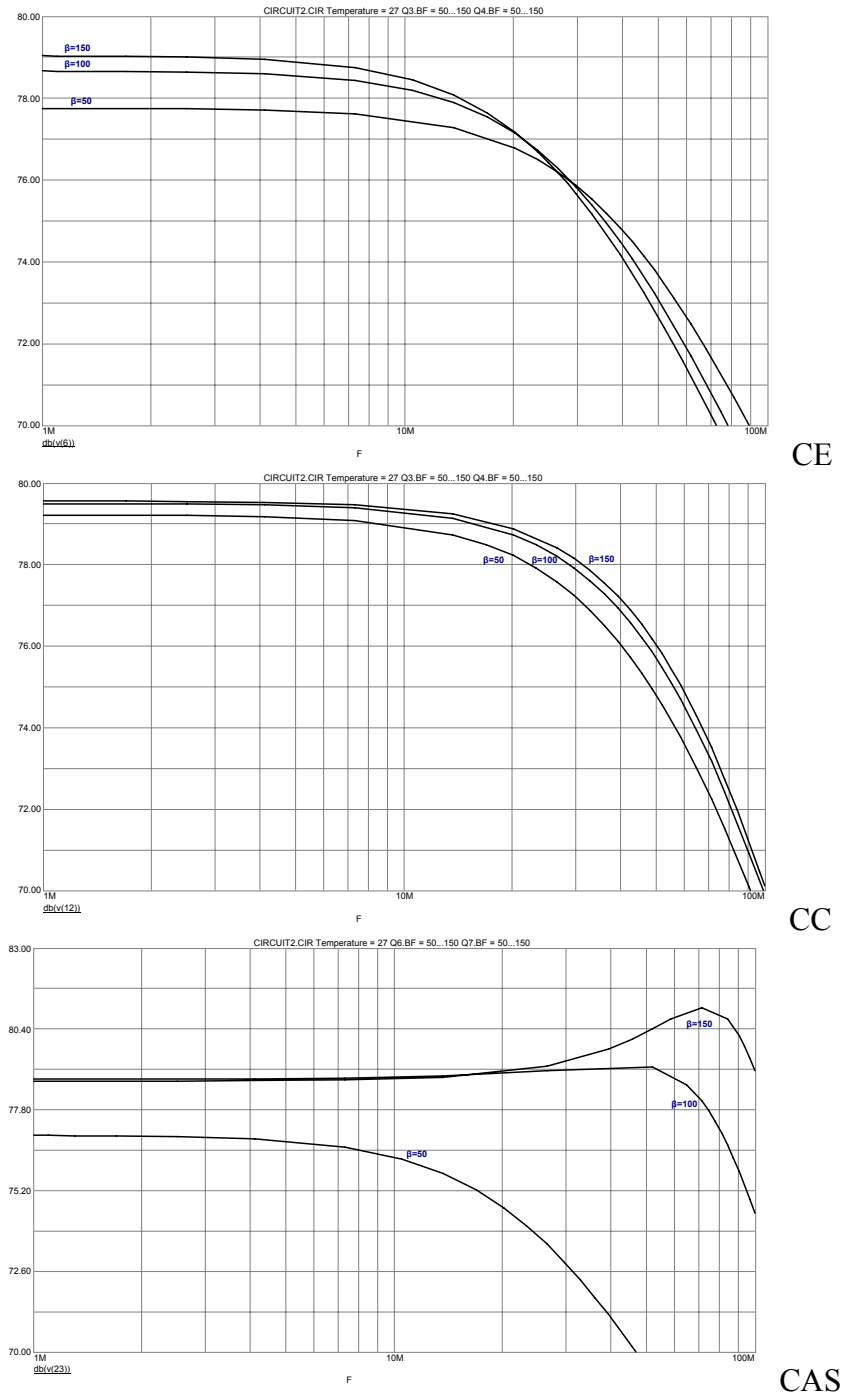

Figure 25. Effect of the variation of β for values 50, 100 and 150 on the preamplifiers behavior

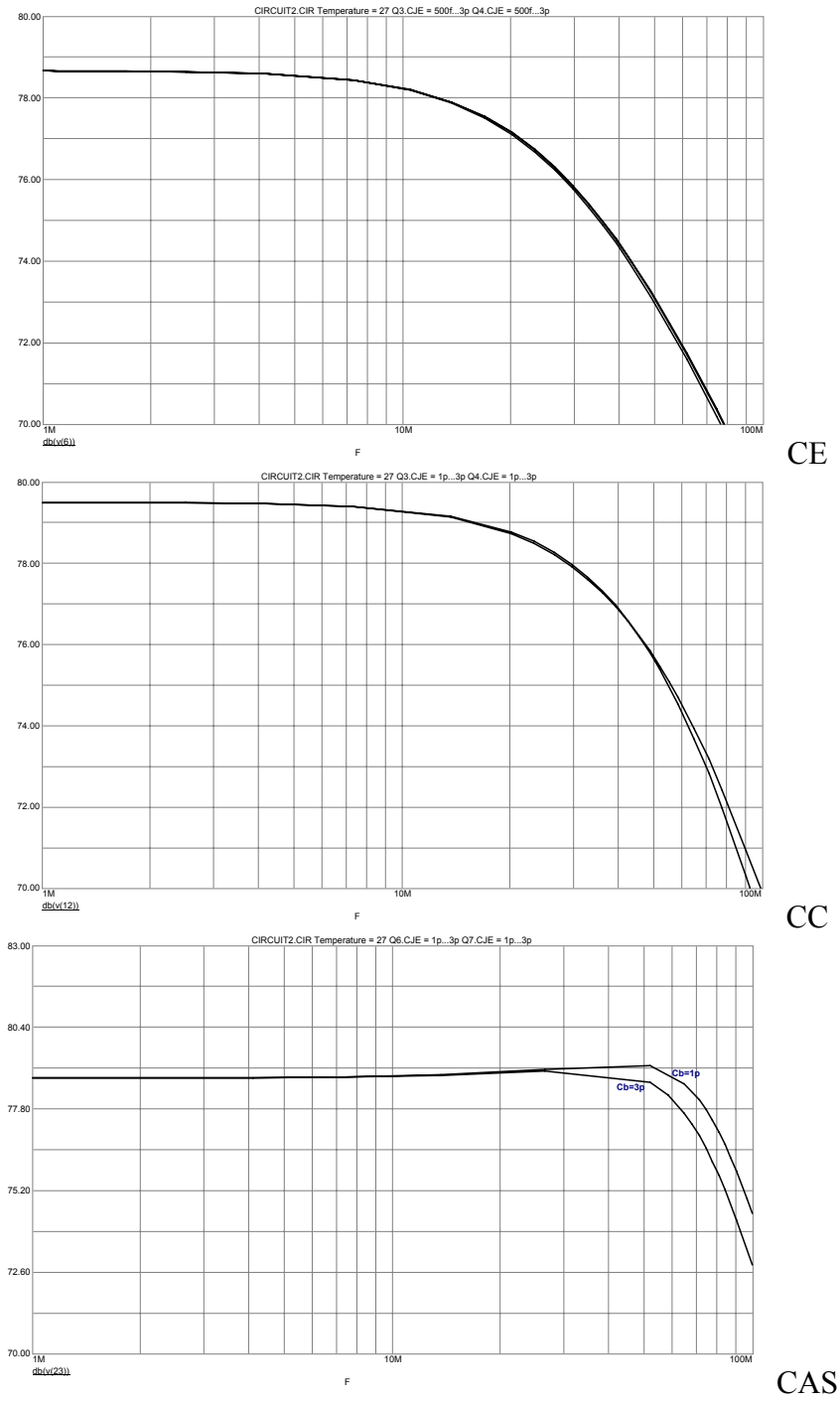

Figure 26. Influence of the variation of C_b for 1pF and 3pF over the stability of the three circuits

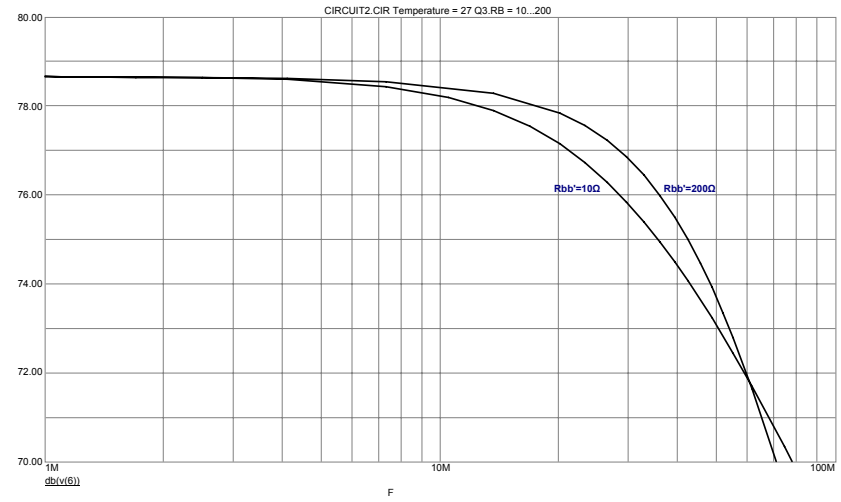

CE

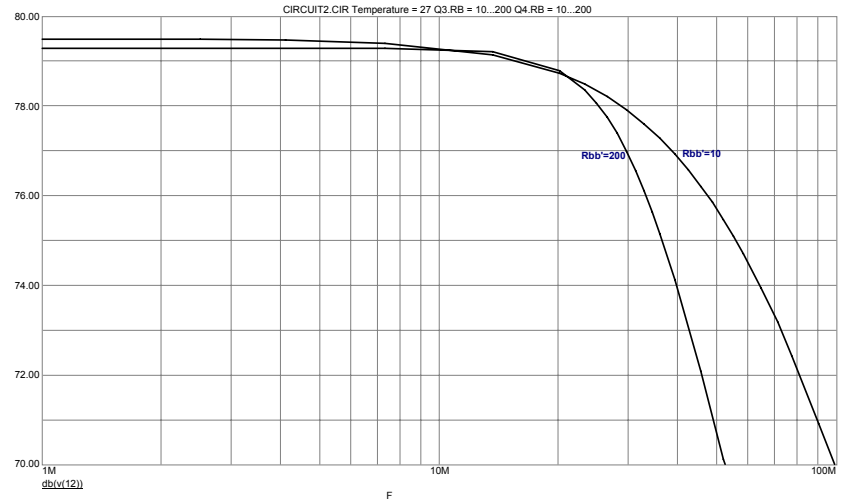

CC

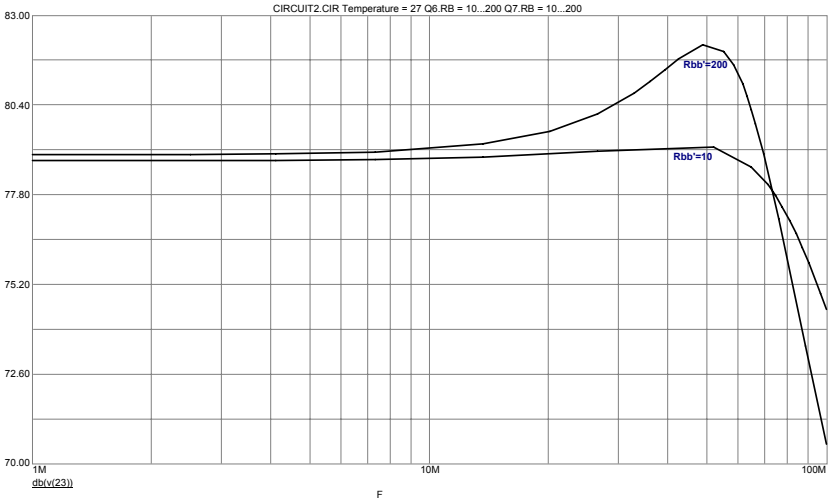

CAS

Figure 27. Influence of $r_{bb'}$ for 10Ω and 200Ω over the stability of the three circuits

3.5.4 INFLUENCE OF THE Cc CAPACITANCE OVER THE BANDWIDTHS OF THE THREE CIRCUITS

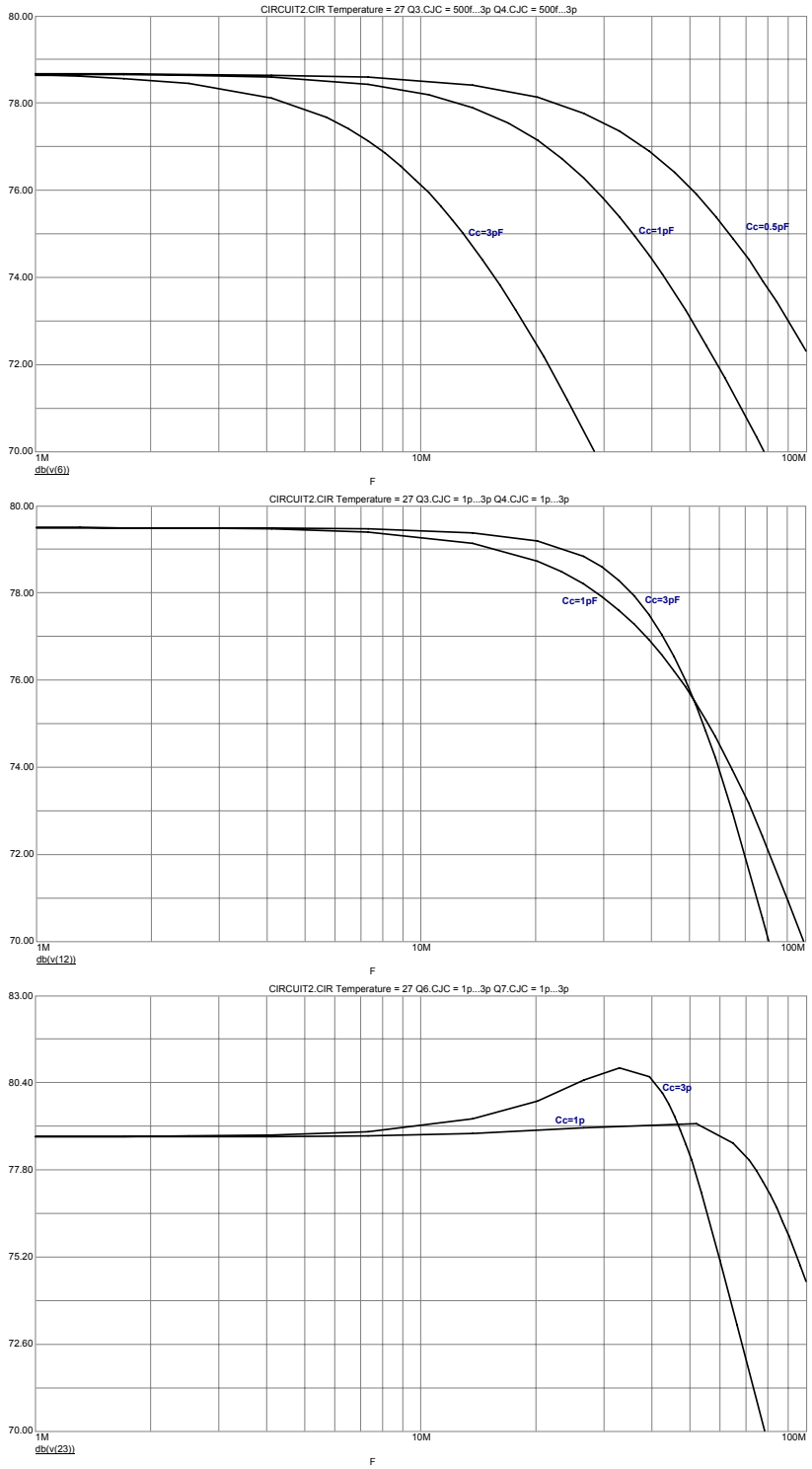

Figure 28. Influence of the Cc capacitance for 0.5pF, 1pF and 3pF over the bandwidth and the stability of the circuits.

Under the view point of bandwidth the most affected circuit appears to be the common emitter followed by the cascode. Regarding the stability, once more the cascode seems to be the circuit which is on the edge of the knife. Indeed an

augmentation of the C_c capacitance pushes the ω_{c2} pole of the transmittance function closer to ω_{c0} (i.e. increases the feedback in frequencies close to the cutoff) creating an important overshoot.

3.5.5 INFLUENCE OF THE TEMPERATURE VARIATIONS OVER THE BEHAVIOUR OF THE CIRCUITS

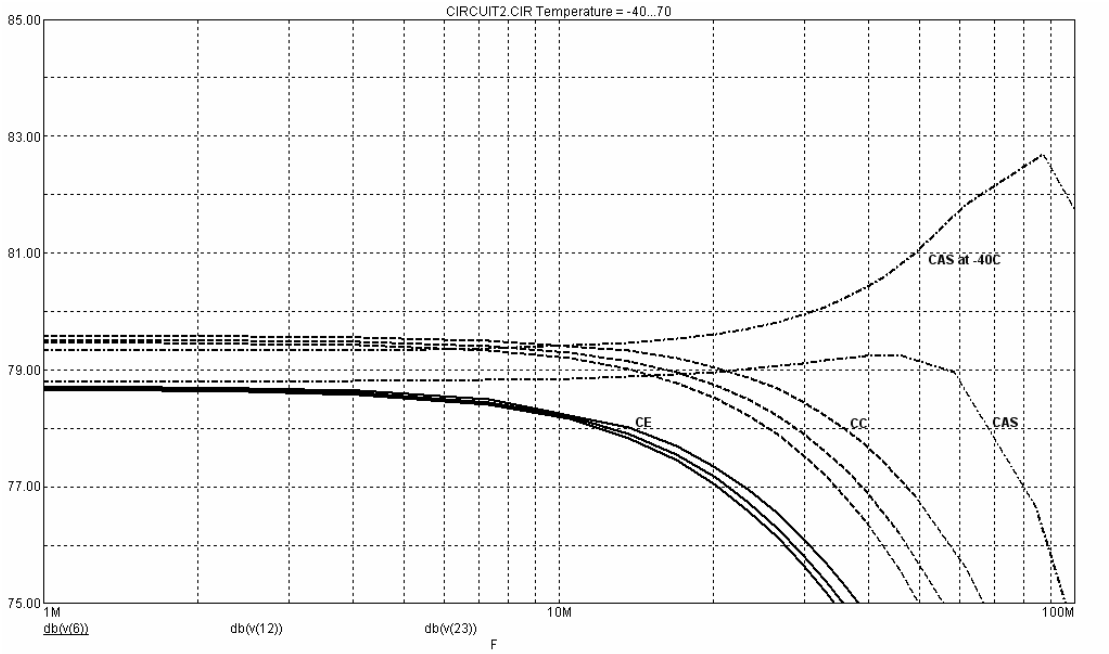

Figure 29. The cascode circuit does not tolerate low operating tempperatures.

Since the circuit is called to make a part of an avionic communication system it has to comply to some very strict operational conditions, meaning that it must be operational over a temperature range 0f -40^0C to $+70^0$C. This requirement is not only a formal one but has a substantial importance since the temperature decrease with a lapse rate of -1.8^0C/1000ft. This means that during a spring day when the temperature at sea level is 20^0C, in an altitude of only 10000fts (roughly 3000m) the environmental temperature will be almost 2^0C The simulation and experimental results show that the common emitter and the common collector circuits have a satisfactory behavior, in the contrary of the cascode which is driven fast toward the instability. For this particular case transient responses are particularly meaningful

.

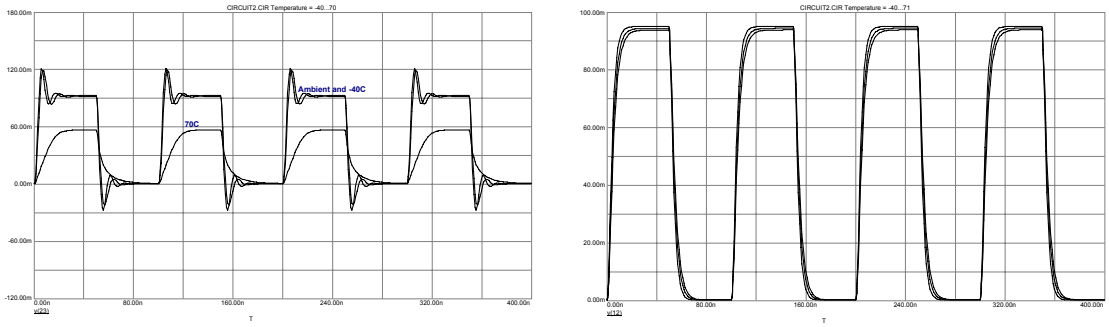

Figure 30. Transient responses over a wide temperature range of the cascode and of the common collector circuits.

Indeed figure 30 displays clearly that the cascode's bandwidth deteriorates toward high temperatures and creates overshoot peaks in low temperatures. In the contrary, the common collector's response appears to be practically insensitive in the temperature window of interest.

3.5.6 EXPERIMENTAL PROTOTYPE AND FLIGHT TEST

Two experimental prototypes have been assembled. The Δ modulator operating at 32KHz is the core of the system (figure 31). The voice commands after being digitized by the Δ modulator are transmitted by a laser diode (850nm, 200mW) with photodiode feedback, which is driven by a specialized laser driver circuit. The received signal after being amplified by a CC amplifier it is passed thru a Δ modulator, which converts the voice commands to analog signal, which drive a loudspeaker. A large surface photodiode (12.5mm^2 of photosensitive area) has been selected in order to increase the S/N. Since the large photosensitive area would lead to large junction capacitance C_d the photodiode has been biased with 60Vdc. An interferential filter is covering the PIN photodiode allowing passing the wavelength band of 800 – 900nm. The receiver optics is simple design with field of views of 30^0. The transmitter optics is a beam expander which has been designed in a way to slightly widen the laser beam to field of view of 10^0 in order to avoid pointing problems during the flight test.

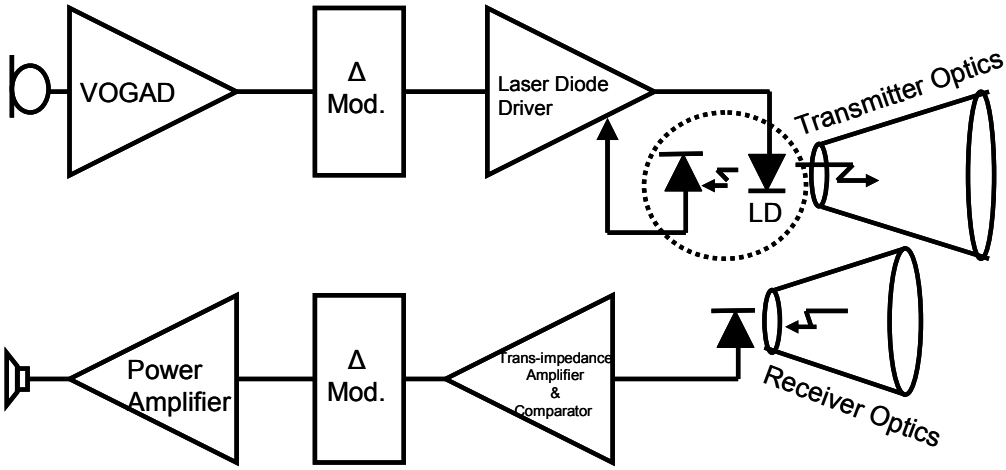

Figure 31. Experimental prototype for the flight test

The test has been carried in two phases. The first phase was a go – no go test at a distance of 100m in the field before the flight. After the successful establishment of voice link the systems have been mounted in two TB9 single engine low wing airplanes. One system has been installed in the starboard window of the "Trainee's airplane" and the second system has been installed in the port window of the "Instructor's airplane".

After take off both airplanes, gained an altitude of 6000ft, and commenced a side by side straight and level flight, the "trainee's airplane" being in the left of the "instructor's airplane", at a distance approximately of 100m. While trainee's airplane kept the radio navigation aids offline, he performed an ADF approach and a consecutive VOR approach under cross wind condition. Both flights have been performed following the instructions of the instructor's airplane thru the IR comm. – link.

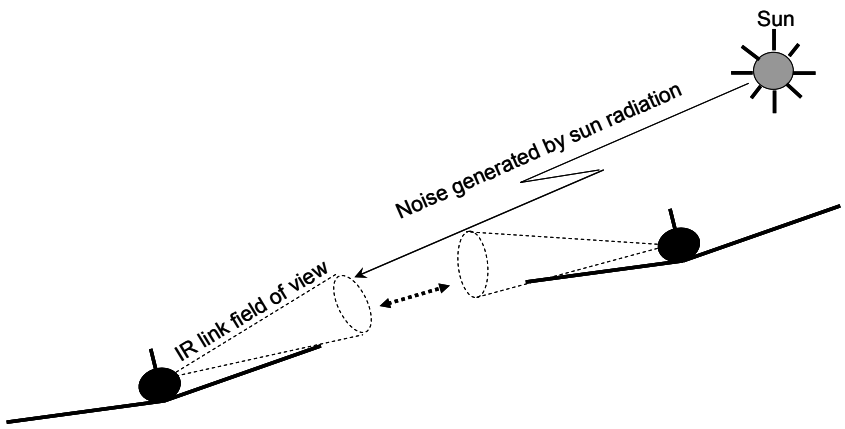

Figure 32. Part of the flight test in order to investigate the sun's effect on the IR comm – link

In order to investigate the eventual sun's effect over the IR comm. – link a turning maneuver has been performed while the trainee's airplane trying to keep the sun inside of the field of view of the receiver. During this final trial the communication continued to be satisfactory despite an detectable rise of background noise.

4. CONCLUSIONS

The research has been investigated the physical layer concerns of an IR communication link for airplanes flying in formation. The following conclusions have been reached:

a. The Sun is the most important noise source for the link and its effects must be limited by all means.

b. The communication can be established only if the atmospheric conditions are such that the airplanes are in visibility range.

c. The common collector trans-impedance amplifier front end is the most adequate trade – off for good stability over wide temperature ranges, good noise performance and good insensitivity to technology variations.

d. As initial approach the link appears to be operationally exploitable and a useful asset for airplanes flying in formation.

e. The laser diodes have a much more limited operating temperature range then that required for avionics applications (-10^0C - $+40^0$C) and therefore a temperature conditioning system for the laser diode must be envisaged for a full scale development.

f. The experimental design was based on a directive beam. However prior a full scale design a transmission system emitting and receiving all around the entire sphere covering the aircraft must be meticulously investigated. This means that the received optical flux will be reduced significantly. Therefore detailed power budget analysis will be mandatory.

g. More powerful laser diodes (1W for instance) on an array have to be envisaged in order to increase the received flux. Also an APD can be used as a substitution to the large surface PIN photodiode for increasing the S/N.

h.Finally a direct sequence spread spectrum system can be established just spreading the Δ modulated signal in order to exploit the process gain of the DSSS improving the S/N.

REFERENCES

[1] Fr. Gfeller, U. Bapst, "Wireless In-house Data Communications via Diffuse Infrared Radiation", Proc. of IEEE, vol.67, No.11, Nov.1979, pp.1474 – 14876

[2] K. Pahlavan, "Wireless Communications for Office Information Networks", IEEE Communication Magazine, Vol. 23, No. 6, June 1985, pp.19 – 27

[3] M. Orgeret, "Les Piles Solaires, le Composant et ses Applications", Masson, 1985, pp. 11 – 24

[4] W. Wolfe, G Zissis, "The Infrared Handbook", Ch. 4 – 6, The Infrared Information and Analysis Center – Environmental Research Institute of Michigan, 1978

[5] R. Hudson Jr., "IR System Engineering", Willey Interscience, Ch. 4.

[6] M. J. N. Sibley, R. T. Unwin, D. R. Smith, "The Design of PIN Bipolar Transimpedance Preamplifiers for Optical Receivers", Journal of the Institution of Electronic and Radio Engineers, Vol. 55, No. 3, pp. 104 – 110, March 1985

[7] M. Aiki, "Low Noise Optical Receiver for High Speed Optical Transmission", Journal of Lightwave Technology, Vol. LT-3, No. 6, pp. 1301 – 1306, December 1985

[7] A. F. Mitchel, M. J. O'Mahoney, "The Performance, Analysis if PIN Bipolar Receivers", Br. Telecom Technology J., Vol. 2, No. 2, pp. 74 – 85, April 1984

[8]M. H. El-Diwany, D. J. Roulston, S. G. Chamberlain, "Design of Low Noise Bipolar Transimpedance Preamplifiers for Optical Receivers", IEE Proc., Vol. 128, Pt. G, No. 6, pp. 299 – 305, December 1981

[9] R. T. Unwinn, "High Speed Optical Receiver", Optical and Quantum Electronics, Vol. 14, pp. 61 – 66, 1982

[10] S. Moustakas, J. L. Hullett, T. D. Stephens, “Comparison of BJT and MESFET Front Ends in Broadband Optical Transimpedance Preamplifiers, Optical and Quantum Electronics, Vol. 14, pp. 57 – 60, 1982

[11]B. Wilson, I. Darwazeh, Umist, “Transimpedance Optical Preamplifier With a Very Low Input Resistance”, Electronic Letters, Vol. 23, No. 4, pp. 138 – 139, February 1987

[12] M. J. N. Sibley, R. T. Unwin, “Transimpedance Optical preamplifier Having a Common Collector Front End”, Electronic Letters, Vol. 18, No. 23, pp. 985 – 986, November 1982

[13] A. F. Mitchell, M. J. O’Mahoney, B. A. Boxall, “PIN Bippolar Optical Receiver Using a High Frequency High Beta transistor”, Electronic Letters, Vol. 19, No. 12, pp. 445 – 447, June 1983

[14] M. J. N. Sibley, R. T. Unwin, D. R. Smith, B. A. Boxall, R. J. Hawkins, “A Monolithic Transimpedance Preamplifier, for High Speed Optical Receivers”, Br. Telecom Technology J., Vol. 2, No. 3, pp. 64 – 66, July 1984

[15] S. Personick, “Receiver Design for Optical Fiber systems”, Proc. of IEEE, Vol. 65, No. 12, pp. 1670 – 1678, December 1977

[16] S. Personick, “Receiver Design for Digital Fiber Optic Communication Systems”, Part I and II, Bell Systems Technical Journal, , Vol. 52, No. 6, pp. 843 – 886, 1973